Energies **2009**, *2*, 71-96; doi:10.3390/en2010071

OPEN ACCESS

energies

ISSN 1996-1073

www.mdpi.com/journal/energies

Article

Analysis of the Coupling Behavior of PEM Fuel Cells and DC-DC Converters

Markus Grötsch [1,⋆], **Michael Mangold** [1] **and Achim Kienle** [1,2]

[1] Max Planck Institute for Dynamics of Complex Technical Systems, Process Synthesis and Process Dynamics Group, Sandtorstraße 1, 39106 Magdeburg, Germany

[2] Otto-von-Guericke-Universität Magdeburg, Lehrstuhl für Automatisierungstechnik / Modellbildung, Universitätsplatz 2, 39106 Magdeburg, Germany

⋆ Author to whom correspondence should be addressed; E-mail: groetsch@mpi-magdeburg.mpg.de.

Received: 8 January 2009 / Accepted: 19 February 2009 / Published: 4 March 2009

Abstract: The connection between PEM fuel cells and common DC-DC converters is examined. The analysis is model-based and done for boost, buck and buck-boost converters. In a first step, the effect of the converter ripples upon the PEM fuel cell is shown. They introduce oscillations in the fuel cell. Their appearance is explained, discussed and possibilities for their suppression are given. After that, the overall behaviors of the coupled fuel cell-converter systems are analyzed. It is shown, that neither stationary multiplicities nor oscillations can be introduced by the couplings and therefore separate control approaches for both the PEMFC and the DC-DC converters are applicable.

Keywords: PEM fuel cell; DC-DC converters; analysis; ripple; oscillations.

1. Introduction

Fuel cells are a promising technology for electrical power generation. They are able to convert chemical energy directly into electrical energy, avoiding an intermediate step of producing mechanical energy. Therefore, the electrical efficiency of fuel cells is considerably higher than that of most conventional processes for electrical power generation. For mobile applications, Polymer-Electrolyte-Membrane fuel cells (PEMFCs) are most suitable. These cells can be characterized by a high power density, an easy production, a low-temperature operation and a fast response to load changes.

A fuel cell is electrically connected to its load via a power conditioning unit (PCU) [1]. This is done

for the purpose of power transfer and power conversion. A PCU is generally made up from storage units and/or conversion units and is typically designed and operated according to requirements and characteristics of the load. While storage units buffer electrical energy, conversion units or converters are used to adapt the DC electricity from the fuel cell to the load's demands. Two types of converters are suitable in fuel cell operation: DC-DC and DC-AC converters.

If a fuel cell is connected to a load via a PCU a complex dynamic system is created. Such a connection might lead to phenomena like multiplicities or oscillations, which are not present in the single systems. These phenomena can contribute to the performance of the whole system either in a positive or in a negative way. Therefore, a detailed investigation of the coupling is necessary to adapt and improve the design and operation of the whole system, especially if the original design was based on single separate subsystems. The coupling behavior of PEMFCs and PCUs is a current field of research. First results have been obtained for the coupling of PEMFCs and DC-AC converters [1–3]. The coupling of these systems leads to a ripple in the fuel cell current at a frequency that is twice the output frequency of the converter. This effect was analyzed in [1–3] and may contribute to fuel cell degradation. In [4] the control of a PEMFC connected to a buck-boost converter was investigated. The emphasis was on converter control and the coupling phenomena were hardly considered. This work tries to extend the results in literature by analyzing the coupling phenomena between PEMFCs and DC-DC converters.

The contribution is divided in 5 sections. In the next section the used PEMFC model is presented. After that the DC-DC converter models are stated. In the following section the results of the analysis are shown. The contribution ends with a conclusion.

2. Modeling of the PEM fuel cell

In this contribution we use a dynamic, lumped one-phase fuel cell model. The main model characteristics are:

- It is assumed that there is no liquid water in the gas bulks and the diffusion layers.
- Only the cathode of the fuel cell is considered. The anodic reaction is assumed to be in equilibrium and the anodic overpotential is equal to zero.
- The cathodic gas bulk and gas diffusion layer are modeled as one perfectly mixed phase (Figure 1).
- The cathodic catalyst layer and the membrane are modeled by the equivalent electrical circuit in Figure 1, as was suggested in [5].
- The dynamic behavior of the membrane's water household is neglected.
- The model is isothermal and the gas phases are isobaric and behave like an ideal gases.
- The Tafel approach is used for the cathode kinetics.

In the following the model equations are presented. For a derivation of the model equations please see Appendix A. The appearing quantities and their values and units are listed in the nomenclature at the end of this article. The parameters for the fuel cell model are mainly taken from [6], while the parameters for

Figure 1. Modeling approach for the PEM fuel cell.

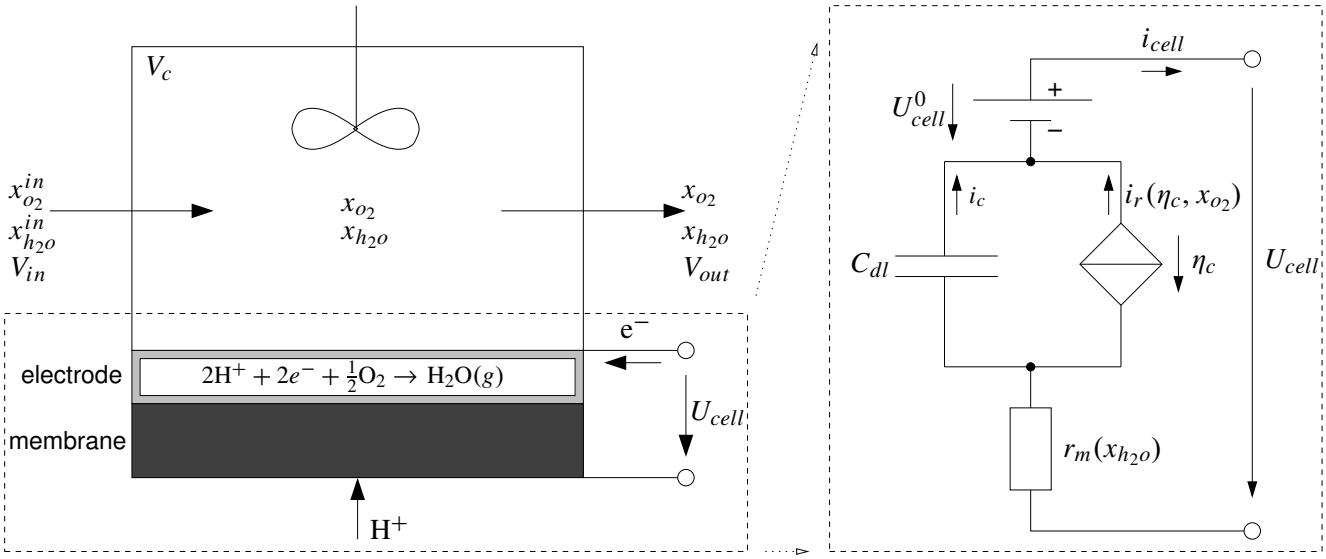

the DC-DC converters are chosen according to guidelines in [7, 8]. First of all, the dynamic equations of the model are specified:

$$V_c\,\dot{x}_{o_2} = -\hat{q}(1 + x_{o_2})\,i_r + (x_{o_2}^{in} - x_{o_2})\,V_{in}, \tag{1}$$

$$V_c\,\dot{x}_{h_2o} = \hat{q}(2 - x_{h_2o})\,i_r + (x_{h_2o}^{in} - x_{h_2o})\,V_{in}, \tag{2}$$

$$C_{dl}\,\dot{\eta}_c = i_r - i_{cell} \quad \text{with} \quad i_r := i_r^0\,x_{o_2}\,\exp(-\hat{\alpha}\eta_c) \tag{3}$$

$$\text{and} \quad \hat{q} := A_g/2c_tnF, \quad \hat{\alpha} := (1-\alpha)nF/R\Theta\,. \tag{4}$$

The differential equations (1) and (2) are used to calculate the content of oxygen x_{o_2} and water vapor x_{h_2o} in the PEMFC. The symbol η_c denotes the overpotential at the cathodic catalyst and is calculated from Eqn. (3). The electrical current density in the fuel cell is given by i_{cell}. V_{in} describes the volume flow rate of humidified air that enters the cell. The other terms are constant model parameters. An additional algebraic equation is used to calculate the cell voltage U_{cell}:

$$U_{cell} = U_{cell}^0 + \eta_c - r_m(x_{h_2o})\,i_{cell}\,. \tag{5}$$

Equation (5) includes activation losses of the catalyst via η_c and ohmic losses in the cell voltage via the resistance r_m of the membrane for proton transport. The membrane's resistance is calculated from its proton conductivity σ_p: $r_m(x_{h_2o}) := d_m/\sigma_p(x_{h_2o})$ where the following dependency from [9] is used:

$$\sigma_p(x_{h_2o}) = \sigma_{p_0}\,exp(14\,(x_{h_2o}\,p_g/p_{sat})^{0.2})\,.$$

In summary, the fuel cell model is made up by a system of 3 nonlinear ordinary differential equations and an additional algebraic equation. The PEMFC model is operated at one-phase conditions with respect to the water household and at a common operating temperature of $\Theta = 353K$ [10]. It is fed with air and will be operated in rheostatic mode due to the coupling with the DC-DC converters. Although this fuel cell model is relatively simple and consists only of a single cell with a cross-sectional area of one square centimeter [6, 11], the modeling approach is complex enough to analyze and outline the essential qualitative effects due to the coupling between one-phase or two-phase PEM fuel cells and DC-DC converters as we will show during the analysis.

3. Modeling of the DC-DC converters

The purpose of DC-DC converters is the transformation of direct electricity. They are built up from power electronic devices and operated as switched systems. Due to the switched operation the output quantities of these systems show an unavoidable ripple which should be small. Three DC-DC converters are considered in this contribution: boost, buck and buck-boost converter [7]. The converters are assumed to be lossless and are modeled with resistive loads. In order to examine the coupling effects between PEMFC and converters due to switching, the DC-DC converters are modeled via switched differential equations. In the case of the boost converter (Figure 2) they read:

$$L\,\dot{I}_l = U_e - (1-s)\,U_c \tag{6}$$

$$C\,\dot{U}_c = (1-s)\,I_l - U_c/R_L \tag{7}$$

where I_l is the inductor current, U_c the capacitor voltage and s is the switching function shown in Figure

Figure 2. Lossless boost converter with resistive load.

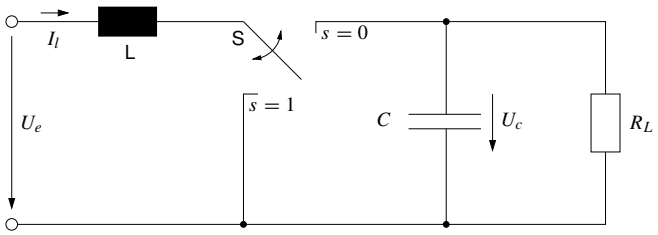

3. The load resistance R_L is assumed to be constant over one switching period T. Note that the input current of the converter, denoted with I_e is equal to the inductor current: $I_e = I_l$. Another widely used

Figure 3. Duty cycle of the DC-DC converters.

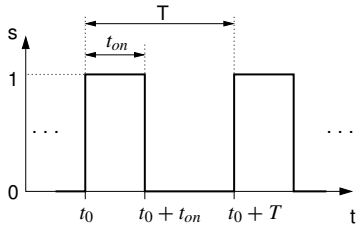

DC-DC converter is the buck converter (Figure 4). It can be modeled with the following equations:

$$L\,\dot{I}_l = s\,U_e - U_c \tag{8}$$

$$C\,\dot{U}_c = I_l - U_c/R_L \tag{9}$$

where I_l is denotes the converter's inductor current and U_c its capacitor voltage. The switching function s is the same as for the boost converter (Figure 3). The input current I_e to the converter in this case is equal to: $I_e = s\,I_l$. The buck-boost converter (Figure 5) is the last considered converter and can also be

Figure 4. Lossless buck converter with resistive load.

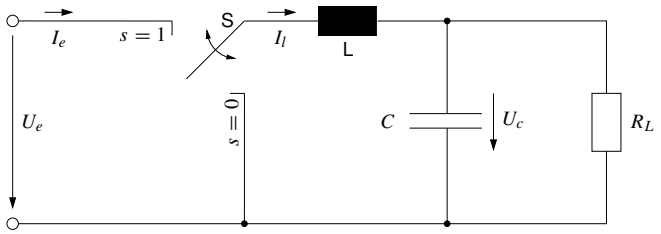

modeled by switched differential equations:

$$L\,\dot{I}_l = s\,U_e + (1-s)\,U_c \tag{10}$$

$$C\,\dot{U}_c = -(1-s)\,I_l - U_c/R_L\,. \tag{11}$$

Again, the inductor current of the converter is denoted by I_l, the capacitor voltage by U_c and the switching function s is given by Figure 3. For the input current I_e the same statement as for the buck converter is true: $I_e = sI_l$.

Figure 5. Lossless buck-boost converter with resistive load.

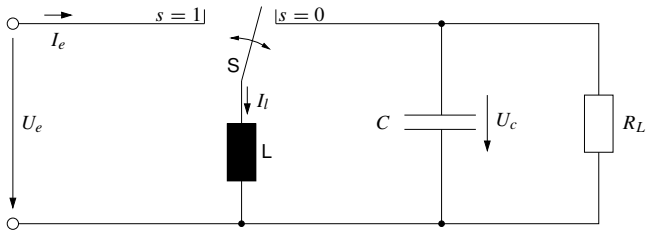

DC-DC converters can also be described by averaged model equations [7] if the intrinsic ripple is negligible. The structure of these equations is the same as for the switched models, only the time-dependent quantities are substituted with their averaged counterparts, where the average is taken over one duty cycle T, i.e.

$$\left[a(t_0)\,,\,\overline{I}_l(t_0)\,,\,\overline{U}_c(t_0)\,,\,\overline{U}_e(t_0)\right] := \frac{1}{T}\int_{t_0}^{t_0+T}\left[s(t)\,,\,I_l(t)\,,\,U_c(t)\,,\,U_e(t)\right]\,dt \tag{12}$$

and the input current I_e is also integrated to be $\overline{I}_e(t_0) = \overline{I}_l(t_0)$ for the boost and $\overline{I}_e(t_0) = a(t_0)\,\overline{I}_l(t_0)$ for the buck and buck-boost converter. The averaged model equations allow a simple characterization of the specified DC-DC converters in terms of their input/output behavior. In Figure 6a the stationary output voltages $\overline{U}_c$ of the three converters are shown. One can see, that a boost (buck) converter can be used to produce an output voltage U_c that is greater (smaller) in magnitude than the input voltage U_e. The buck-boost converter is a mixed form and is used to invert the output voltage U_c and decrease or increase its magnitude with respect to the input voltage U_e. In Figure 6b the stationary input resistances of the converters $\overline{R}_e := \overline{U}_e/\overline{I}_e$ are depicted.

Figure 6. Stationary and averaged output voltages $\overline{U}_c$ (a)and input resistances $\overline{R}_e$ (b) of boost, buck and buck-boost converters with respect to their duty ratio a.

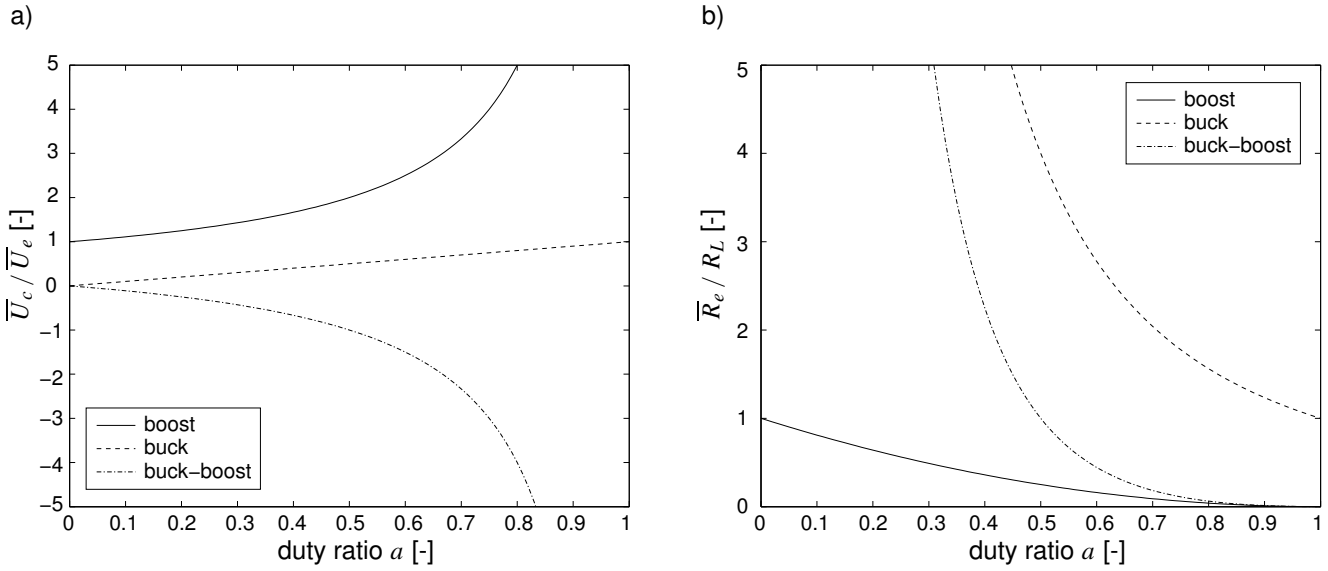

4. Interconnection analysis of PEMFC and DC-DC converters

In this section the connection between PEMFC and DC-DC converters is analyzed. First of all, the coupling conditions are specified. For the coupling between the PEM fuel cell (Eqns. (1-5)) and the converters (Eqns. (6-11)) the following conditions apply:

$$U_{cell} \triangleq U_e \quad \text{and} \quad i_{cell} \triangleq I_e/A_g\,. \tag{13}$$

With the above equation the fuel cell and the converters are connected and a feedback of the converter's input current I_e to itself via the cell voltage U_{cell} (Eqn. (5)) is established. It is the aim of this contribution to analyze the effect and extent of this feedback. This is done for each connection in three steps. In a first step, the effect of the converter ripple upon the PEMFC is shown and explained, while in the second step the found effect is discussed. Finally, the overall behavior of the connected PEMFC - converter system is examined in order to check for the appearance of stationary multiplicities and oscillations due to the coupling.

4.1. PEMFC and Boost-converter

In this section the coupling between the PEMFC and the boost converter is examined.

Effect of the converter ripple upon the PEMFC In a first step the effect of the converter ripple upon the PEMFC is shown. For this purpose the PEMFC (Eqns. (1-3)) and the boost converter model (Eqns. (6,7)) are coupled via Eqn. (13) and form a system of switched differential equations. This system is dynamically simulated using step changes of the load resistance R_L depicted in Figure 7. The converter's duty ratio a is set to 0.2 and the other model parameters are kept constant at their nominal values. Three simulations I, II, III are performed with the same initial value R_L^I. In simulation I the load resistance is kept constant at R_L^I whereas in simulations II and III the load is stepped to R_L^{II} and R_L^{III} respectively.

Figure 7. Time plot of load resistance R_L and stationary voltage-current profile of the PEM fuel cell with assigned operating points.

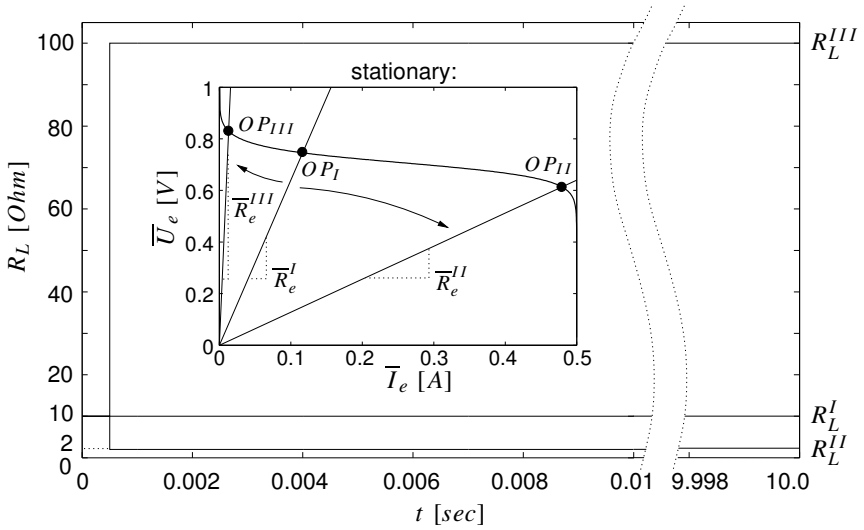

The simulation scenario can be further illustrated with the stationary voltage-current profile of the PEMFC together with the considered operating points OP_I, OP_{II} and OP_{III} shown inside of Figure 7. The operating points are determined by the load resistance R_L. A relationship between $\overline{R}_e$ and R_L^i can be derived from the averaged version of the boost converter model in Eqns. (6,7):

$$L\,\dot{\overline{I}}_l(t_0) = \overline{U}_e(t_0) - (1 - a(t_0))\,\overline{U}_c(t_0)$$
$$C\,\dot{\overline{U}}_c(t_0) = (1 - a(t_0))\,\overline{I}_l(t_0) - \overline{U}_c(t_0)/R_L$$

For the stationary operation of the converter one obtains: $\overline{U}_e = (1-a)\overline{U}_c$ and $\overline{I}_l = \overline{U}_c/(1-a)R_L$. The average input resistance of the boost converter is given by $\overline{R}_e = \overline{U}_e/\overline{I}_e$ and with the dependency $\overline{I}_e = \overline{I}_l$ one obtains from the previous statements $\overline{R}_e = R_L(1-a)^2$.

The simulation results are shown in Figures 8 and 9. The diagrams are split into two parts. The first part shows the time plots from the simulation start to the settlement of the electrical transients of the coupled system. The second part shows stationary simulations after the transients for mass transport of oxygen and water vapor have settled. It can be seen, that during simulations I and II no significant impact from the PEMFC to the boost converter or vice versa can be found. After the applied step the simulation settles and finally reaches a steady state. The oscillations of the quantities are small and can be neglected. In contrast, if simulation III is considered a clear interaction of PEMFC and converter can be observed. The overpotential η_c and the cell voltage U_e in Figure 8 show relatively large oscillations compared to the cases I, II. The oscillations are present immediately after the applied step and also at steady state. This is not the case for the converter input current I_e and the capacitor voltage U_c in Figure 9. Both of them show only small oscillations in case III, similar to the simulation cases I and II. The given interaction is therefore one-sided in direction from boost converter to PEMFC and is located at small cell currents in the activation polarization region of the fuel cell (Figure 7).

The reason for this interaction can be found from the model equation of the overpotential in Eqn. (3). A linearization of this equation at an averaged and stationary operating point $(\overline{x}_{o_2}^s, \overline{x}_{h_2o}^s, \overline{\eta}_c^s, \overline{I}_e^s, \overline{U}_c^s)$ of

Figure 8. a) Step response of overpotential η_c and b) cell (=converter input) voltage U_e.

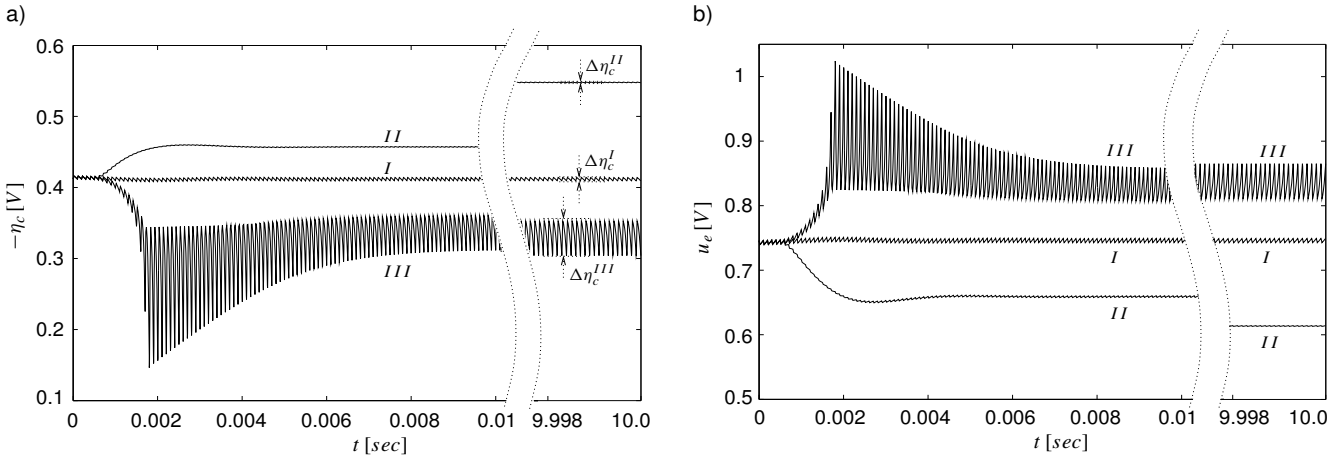

Figure 9. a) Step response of converter input (=inductor) current I_e and b) capacitor (=converter output) voltage U_c.

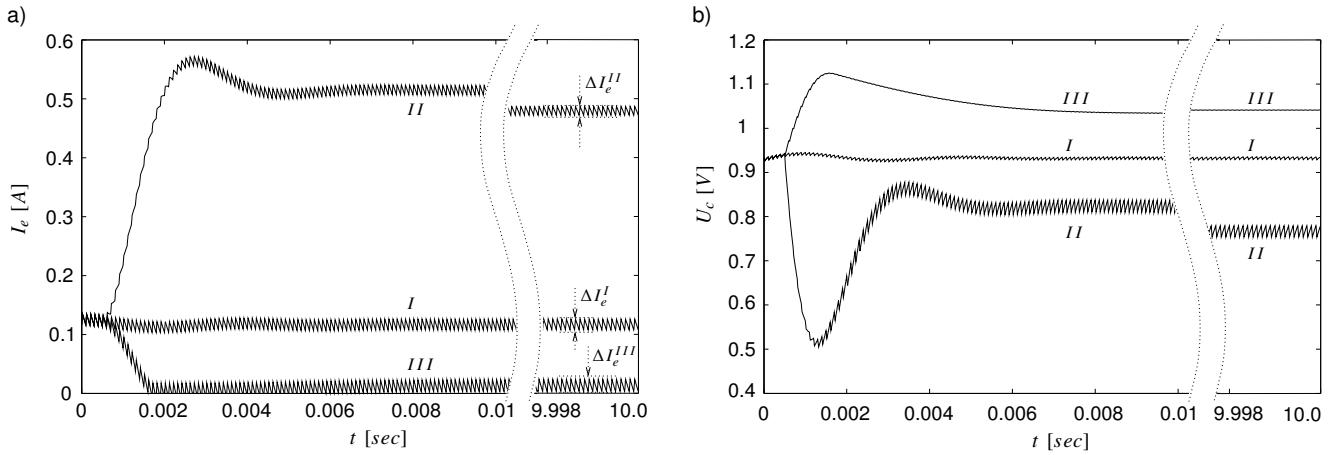

the coupled system leads to

$$\underbrace{\frac{C_{dl}}{\hat{\alpha}\,\overline{I}_e^{\,s}/A_g}}_{\tau:=}\delta\dot{\eta}_c + \delta\eta_c = -\frac{\delta I_e}{\hat{\alpha}\,\overline{I}_e^{\,s}} \tag{14}$$

$$\text{with} \quad \overline{I}_e^{\,s} = A_g i_r^0 \overline{x}_{o_2}^{\,s} \exp(-\hat{\alpha}\overline{\eta}_c^{\,s}) \tag{15}$$

where $\delta\eta_c$ and δI_e are the variations of the overpotential and the converter input current around the operating point respectively. It is assumed, that the variation of the oxygen content x_{o_2} due to the converter switching can be neglected. The variation δI_e of the converter input current is considered as an input quantity in Eqn. (14), which is independent from $\delta\eta_c$ because of the observed one-sided interaction from converter to PEMFC. Equation (14) is therefore a linear ordinary differential equation of first order with constant coefficients whose transient behavior is determined by its time constant τ. If the time constant τ is small compared to the given time interval of the duty cycle T then the variation $\delta\eta_c$ can approximately be calculated by

$$\delta\eta_c \approx -\frac{1}{\hat{\alpha}\overline{I}_e^{\,s}}\delta I_e = -\frac{\partial(-\overline{\eta}_c^{\,s})}{\partial\overline{I}_e^{\,s}}\delta I_e\,. \tag{16}$$

This relationship is determined from the Tafel kinetic in Eqn. (15) where $\partial(-\overline{\eta}_c^{\,s})/\partial\overline{I}_e^{\,s}$ is the sensitivity of the overpotential $-\overline{\eta}_c^{\,s}$ with respect to the cell current $\overline{I}_e^{\,s}$. It can be seen, that the sensitivity increases with decreasing cell current. If the variation δI_e does not change very much at different cell currents $\overline{I}_e^{\,s}$, the change of variation $\delta\eta_c$ can approximately be determined by the changed sensitivity. This is the case for the three simulation experiments above. The oscillations ΔI_e^i, $i = I, II, III$ in the cell current (Figure 9a) are nearly the same for all three simulation cases, but the average values are clearly different. For simulation case III the average cell current is the smallest resulting in the largest sensitivity of the three cases. The large oscillations in the overpotential for case III (Figure 8a) are the consequence. In Figure 10 the above statements are illustrated. The Tafel equation (15), the oscillation amplitudes of the cell current ΔI_e^i (Figure 9a) and the corresponding amplitudes of the overpotential $\Delta\eta_c^i$ (Figure 8a) are shown for the three simulation cases I, II and III.

We have seen, that the reason for the large oscillation $\Delta\eta_c^{III}$ is a too small time constant τ with respect to the duty period T. From Eqn. (14) we can see, that the time constant τ is proportional to the double layer capacitance C_{dl} and (with Eqn. (16)) to the sensitivity $\partial(-\overline{\eta}_c^{\,s})/\partial\overline{I}_e^{\,s}$. The sensitivity in simulation III is the largest, so the double layer capacitance C_{dl} of the fuel cell is responsible for the small τ. Therefore, the oscillations in the activation polarization region of the PEMFC in III are caused by an insufficient adaption of the double layer capacitance C_{dl} and the duty period T to each other.

Discussion of the effect We have shown and explained in the previous section that the converter ripple introduces oscillations in the activation polarization region of the fuel cell. This statement is true for the used double layer capacitance C_{dl} and duty period T, but it is also in general valid as long as the ratio between C_{dl} and T is less or equal to the given one. This means for example, that we cannot increase T in order to decrease switching losses in the boost converter, because this will result in larger oscillations in the fuel cell. This also means for example, that if the fuel cell owns a larger double layer capacitance C_{dl} and we use the same duty period T the oscillations will vanish. If we increase the duty period T (and

Figure 10. Tafel equation for simulation cases I, II and III.

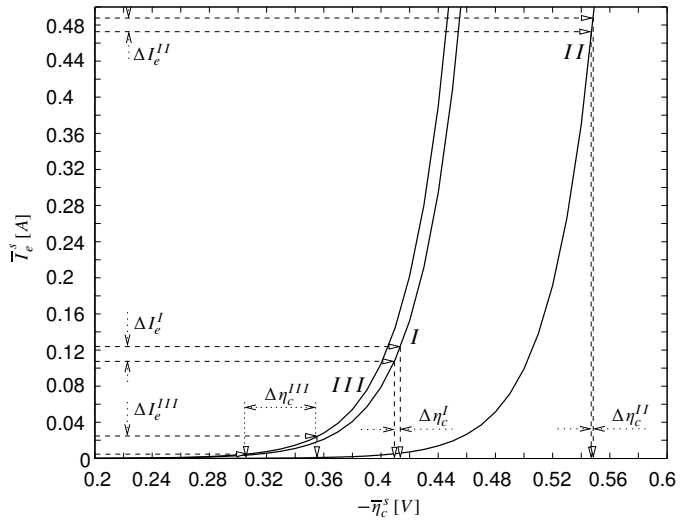

the boost converter's inductivity L, capacitance C to stay at the same ripple in the output voltage U_c) the oscillations will reoccur.

The impact of converter introduced oscillations in the overpotential is currently under research and up to now it is not clear, if they lead to cell degradation, as long as no reactant depletion appears [12]. Anyway, in order to avoid oscillations in the fuel cell we have to take suitable measures which are presented in the following. For the above simulations we used a small double layer capacitance in the order of magnitude as in [13, 14]. In other publications like in [15, 16] a larger double layer capacitance in the PEMFC is observed. For the latter case, the oscillations in the fuel cell vanish for the given duty period and no further effort has to be taken to avoid them. In the first case there are two simple possibilities to avoid oscillations. The first is to decrease the duty period T. This has a smaller variation ΔI_e of the cell current and a larger impact of the time constant τ within the time interval T as a consequence, but can also lead to larger switching losses in the converter. The second alternative is to increase the double layer capacitance C_{dl} of the PEMFC and therefore the time constant τ. The first point can be achieved via the control of the boost converter. After the boost converter has been designed [7] and the duty period T has been adjusted to meet the boost converter's requirements, a minimal cell current $\overline{I}_e^{s,min} \leq \overline{I}_e^s$ has to be specified. This puts an upper bound on the sensitivity in Eqn. (16). If the double layer capacitance and all other necessary parameters are roughly known then the relevant time constant $C_{dl}A_g/\hat{\alpha}\overline{I}_e^{s,min}$ can be estimated. If $T \gg C_{dl}A_g/\hat{\alpha}\overline{I}_e^{s,min}$ oscillations are expected to appear if the fuel cell is operated in the activation polarization region. In order to avoid these oscillations the duty period T can be decreased, e.g. $T \leq C_{dl}A_g/\hat{\alpha}\overline{I}_e^{s,min}$. The second possibility can be implemented for example by inserting a capacitor between PEMFC and boost converter. This leads to an increased double layer capacitance as is shown in appendix B.

Overall behavior of the coupled system With the above suggestions the impact of the converter ripple can be suppressed and we can describe the connection between the PEMFC and the boost converter with averaged model equations and check the overall behavior of this coupled system for the occurrence of

stationary multiplicities and oscillations.

At first, we consider the stationary operation of PEMFC and boost converter. Therefore, the stationary and averaged relationship in Figure 6 for the boost converter is valid. Due to the coupling in Eqn. (13) the input resistance of the converter $\overline{R}_e$ serves as load resistance of the PEMFC $\overline{V}_{cell}/\overline{I}_{cell} = \overline{U}_e\, A_g/\overline{I}_e = \overline{R}_e A_g$ and forces a rheostatic operation of the cell. Moreover, the mapping between the converter's input resistance $\overline{R}_e$ and the load resistance R_L is unique as is indicated in Figure 6b. Therefore, no further stationary multiplicities are added by the coupling PEMFC and boost converter to the ones that are already present in a rheostatic operated PEM fuel cell [17–19].

However, oscillations induced by the coupling are still possible. They appear if a Hopf bifurcation occurs due to the coupling. A Hopf bifurcation appears in a nonlinear system $\dot{\mathbf{z}} = \mathbf{f}(\mathbf{z}, \mathbf{p})$ if a pure imaginary pair of eigenvalues of the Jacobian matrix $\mathbf{J} = \partial\mathbf{f}/\partial\mathbf{z}$, evaluated at the steady state $(\mathbf{z}_0, \mathbf{p}_0)$ arises at the parameter $\mathbf{p}_0$. Therefore, in order to search for the onset of oscillations, we have to check the Jacobian matrix of the coupled system. For this purpose we start with the following averaged model of PEMFC and boost converter:

$$V_c\,\dot{\overline{x}}_{o_2} = -\hat{q}(1+\overline{x}_{o_2})\,\overline{i}_r + (x_{o_2}^{in} - \overline{x}_{o_2})\,V_{in}, \tag{17}$$

$$V_c\,\dot{\overline{x}}_{h_2o} = \hat{q}(2-\overline{x}_{h_2o})\,\overline{i}_r + (x_{h_2o}^{in} - \overline{x}_{h_2o})\,V_{in}, \tag{18}$$

$$C_{dl}\,\dot{\overline{\eta}}_c = \overline{i}_r - \overline{I}_l/A_g \quad \text{with} \quad \overline{i}_r = i_r^0\,\overline{x}_{o_2}\,\exp(-\hat{\alpha}\overline{\eta}_c), \tag{19}$$

$$L\,\dot{\overline{I}}_l = U_{cell}^0 + \overline{\eta}_c - r_m(\overline{x}_{h_2o})\,\overline{I}_l/A_g - (1-a)\,\overline{U}_c, \tag{20}$$

$$C\,\dot{\overline{U}}_c = (1-a)\,\overline{I}_l - \overline{U}_c/R_L. \tag{21}$$

It is derived by coupling Eqns. (1-7) using Eqn. (13) and averaging, like in Eqn. (12), the resulting model over one duty cycle. For this purpose it is assumed that the states $x_{o_2}, x_{h_2o}, \eta_c, I_l, U_c$ are approximately constant during one duty cycle. This is a valid assumption due to the negligible impact of the converter ripple.

The above system of equations includes averaged model equations for oxygen and water transport (Eqn. (17,18)). This mass transport typically shows transient times in the order of magnitude of seconds while the resonant behavior of the converter is in the order of magnitude of milli seconds and smaller. Due to this we consider the mass transport Eqns. (17,18) as static and use only the equations (19-21) to search for the appearance of a Hopf bifurcation.

The first step in order to detect a Hopf bifurcation is the calculation of the Jacobian matrix. If we calculate the Jacobian matrix of equations (19-21) at the steady state $(\overline{x}_{o_2}^{ss}, \overline{x}_{h_2o}^{ss}, \overline{\eta}_c^{ss}, \overline{I}_l^{ss}, \overline{U}_c^{ss}, R_L^{ss}, a_{ss})$ we get

$$\mathbf{J} := \begin{bmatrix} -b_{11} & -b_{12} & 0 \\ b_{21} & -b_{22} & -b_{23} \\ 0 & b_{32} & -b_{33} \end{bmatrix} = \begin{bmatrix} -\hat{\alpha}\overline{I}_l^{ss}/A_gC_{dl} & -1/A_gC_{dl} & 0 \\ 1/L & -r_m(\overline{x}_{h_2o}^{ss})/A_gL & -(1-a_{ss})/L \\ 0 & (1-a_{ss})/C & -1/R_L^{ss}C \end{bmatrix}. \tag{22}$$

The duty ratio a_{ss} of the boost converter is typically between $0 \leq a_{ss} < 1$ and therefore, the coefficients b_{ij} of $\mathbf{J}$ are always greater than zero. In the next step we have to check the location of the eigenvalues of the Jacobian matrix $\mathbf{J}$. The eigenvalues of $\mathbf{J}$ are the roots of the characteristic polynomial $P(\lambda) =$

$det(\lambda \mathbf{I} - \mathbf{J})$ which is given by

$$P(\lambda) = \lambda^3 + c_2\lambda^2 + c_1\lambda + c_0 \tag{23}$$

with

$$c_2 := b_{11} + b_{22} + b_{33}, \tag{24}$$

$$c_1 := b_{11}b_{22} + b_{11}b_{33} + b_{22}b_{33} + b_{23}b_{32} + b_{12}b_{21}, \tag{25}$$

$$c_0 := b_{11}b_{22}b_{33} + b_{11}b_{32}b_{23} + b_{21}b_{12}b_{33}. \tag{26}$$

The location of the roots of $P(\lambda)$ can be determined with the criterion of LIÉNARD-CHIPART [20]. The polynomial has only roots with negative real parts if the following necessary and sufficient conditions are fulfilled: $c_0 > 0,\ c_2 > 0$ and $c_2\, c_1 - c_0 > 0$. The first two conditions are fulfilled through Eqns. (24,26), because the coefficients c_2, c_1 and c_0 of the polynomial are always positive. The third condition is also fulfilled, because of

$$\begin{aligned} c_2c_1 - c_0 = {} & b_{11}^2b_{22} + b_{11}^2b_{33} + b_{11}b_{12}b_{21} + b_{11}b_{22}^2 + b_{11}b_{22}b_{33} + b_{22}^2b_{33} + \\ & b_{22}b_{23}b_{32} + b_{12}b_{21}b_{22} + b_{11}b_{22}b_{33} + b_{11}b_{33}^2 + b_{22}b_{33}^2 + b_{23}b_{32}b_{33} > 0. \end{aligned} \tag{27}$$

Therefore, the characteristic polynomial $P(\lambda)$ (Jacobian matrix $\mathbf{J}$) has always roots (eigenvalues) with negative real parts and because of this the connection between a PEMFC and a boost converter cannot lead to a Hopf bifurcation in the coupled PEMFC - boost converter system.

4.2. PEMFC and Buck-converter

In this section the coupling between the PEMFC and the buck converter is examined.

Effect of the converter ripple upon the PEMFC In the first step we consider the effect of the buck converter ripple upon the fuel cell. For this purpose we couple the PEMFC (Eqns. (1-3)) and the buck converter model (Eqns. (8,9)) with Eqn. (13) and apply step changes of the duty ratio a (Figure 11a) to this system. The load resistance R_L is chosen such that the fuel cell is operated close to the maximum power point. The other model parameters are at their nominal values. Two simulations I, II are carried out. In simulation I the duty ratio a is kept constant at a_I and in II the duty ratio is stepped to a_{II}. The simulation scenario can be further illustrated by the stationary voltage current profile of the fuel cell and the considered operating points OP_I and OP_{II}. It is shown inside of Figure 11a. The operating points are determined by the buck converter's input resistance $\overline{R}_e$ via the converter's duty ratio a from the following dependency $\overline{R}_e^i = R_L/a_i^2$ with $i = I, II$. This relationship can be derived in an analogous manner from an averaged and stationary version of the buck converter model like it was done for the boost converter in section 4.1..

The simulation results are shown in Figures 11b and Figure 12. The diagrams are split into two parts. As in section 4.1., the first part shows the fast dynamics due to electrical effects, the second part shows the long term behavior, after the transients of the mass balances have settled. In simulation I the duty ratio is equal to $a = a_I = 1$. This means that the switch S of the buck converter is always in position $s = 1$ and no oscillations occur. In contrast, if simulation II is considered, relative large oscillations in the overpotential η_c^{II} (Figure 11b), cell current I_e^{II} (Figure 12a) and the cell voltage U_e^{II} (Figure 12b) are appearing. The large oscillations are present immediately after the applied step and also at the steady state. This is not the case for the inductor current I_l^{II} (Figure 12a) and the capacitor voltage U_c^{II} (Figure

Figure 11. a) Time plot of duty ratio a and (inside) the stationary voltage-current profile of the fuel cell with considered operating points. In b) the step response of the overpotential η_c is shown.

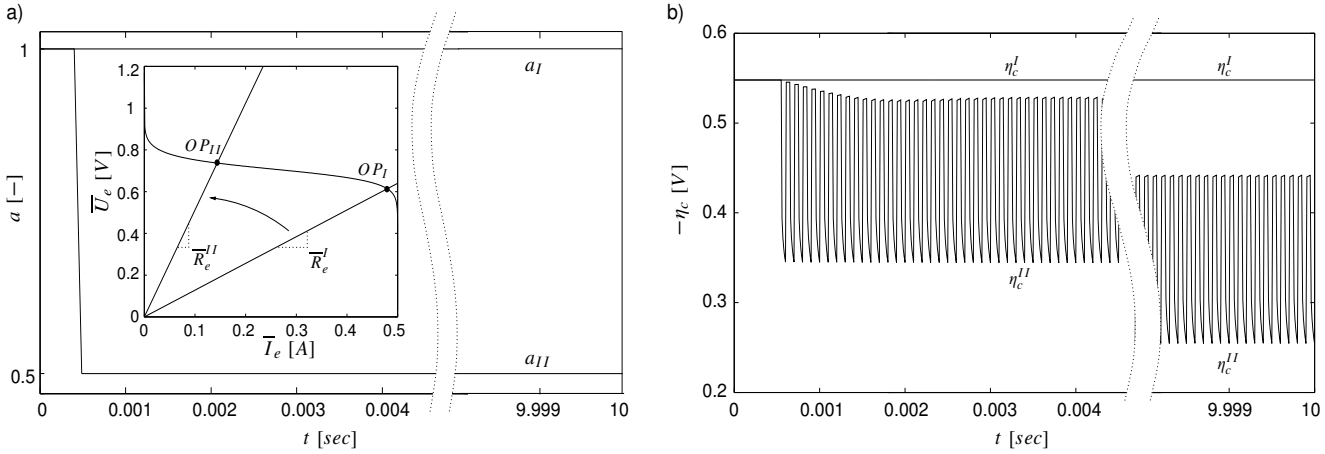

Figure 12. a) Step response of inductor current I_l and cell (=converter input) current I_e. In b) the step responses of cell (=converter input) voltage U_e and capacitor (=converter output) voltage U_c are shown.

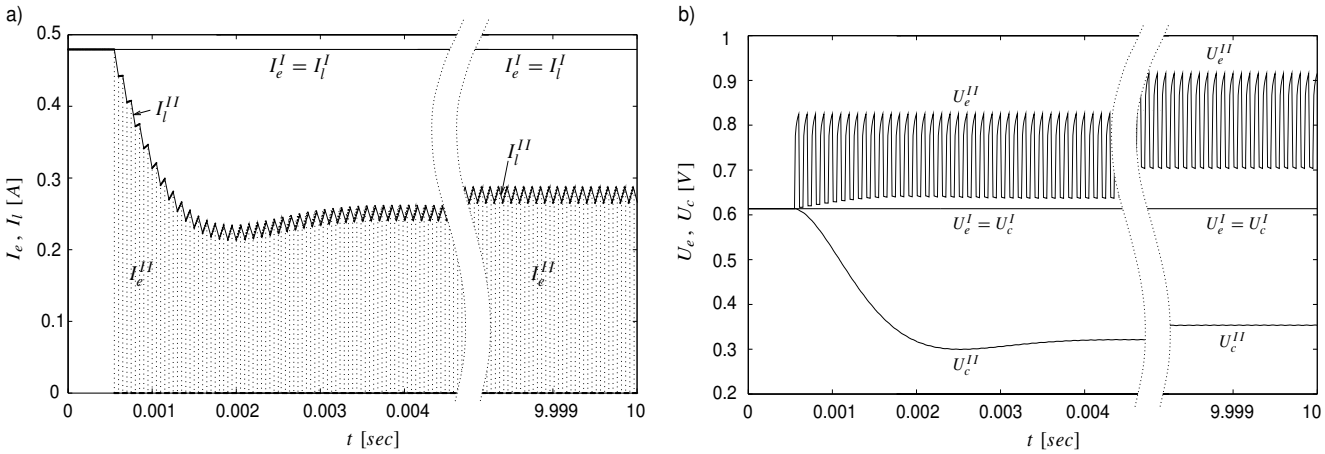

12b) of the converter. Both of them show only small oscillations. The given interaction is therefore one-sided in direction from the buck converter to the PEMFC. The reason for the relatively large oscillations in the PEMFC is due to the presence of the switching function s in the coupling of fuel cell and buck converter: $i_{cell} = I_e/A_g = s\, I_l/A_g$. This leads to a switched ODE for the overpotential:

$$C_{dl}\,\dot{\eta}_c = i_r^0 x_{o_2} \exp(-\hat{\alpha}\eta_c) - s\, I_l/A_g \tag{28}$$

and causes the large oscillations in the overpotential and in the cell voltage.

Discussion of the effect The above equation can be used to further discuss the oscillation amplitudes of the overpotential. With the above observation that the interaction is one-sided from buck converter to the fuel cell and the assumptions that the changes in the inductor current I_l and the oxygen content x_{o_2} are small over one duty period T and can be approximately described by their average values $\overline{I}_l$ and $\overline{x}_{o_2}$, the following formula can be derived for the stationary oscillation amplitudes $\Delta\eta_c$ of the overpotential:

$$\Delta\eta_c = \frac{1}{\hat{\alpha}} \ln\left(1 + \frac{\gamma(1-a)T\left(\frac{\gamma}{\beta}\exp(-\beta a T) - 1\right)}{\frac{\gamma}{\beta}\left(\frac{\gamma}{\beta}\exp(-\beta a T) - 1\right) + \exp(-\beta a T)\left(\frac{\gamma}{\beta} - \gamma(1-a)T\right)}\right) \tag{29}$$

$$\text{with} \quad \gamma = \hat{\alpha}\, i_r^0\, \overline{x}_{o_2} \,/\, C_{dl}\,, \;\; \beta = \hat{\alpha}\, \overline{I}_l \,/\, A_g\, C_{dl} \quad \text{and} \quad (1-a)T\beta > 1\,.$$

The derivation of this equation is given in Appendix C. The equation can be used to further investigate the oscillations in the fuel cell. Figure 13a shows the oscillation amplitudes $\Delta\eta_c$ calculated with Eqn. (29) at different duty ratios a. The ratio of duty period and double layer capacitance T/C_{dl} is used as parameter and the other quantities remain constant at their nominal values. It can be seen, that a

Figure 13. a) Stationary oscillation amplitudes $\Delta\eta_c$ of the overpotential with respect to the buck converter's duty ratio a at different ratios of duty period and double layer capacitance T/C_{dl} and b) stationary simulations of the overpotential for the cases i to iii at a duty ratio $a = 0.5$.

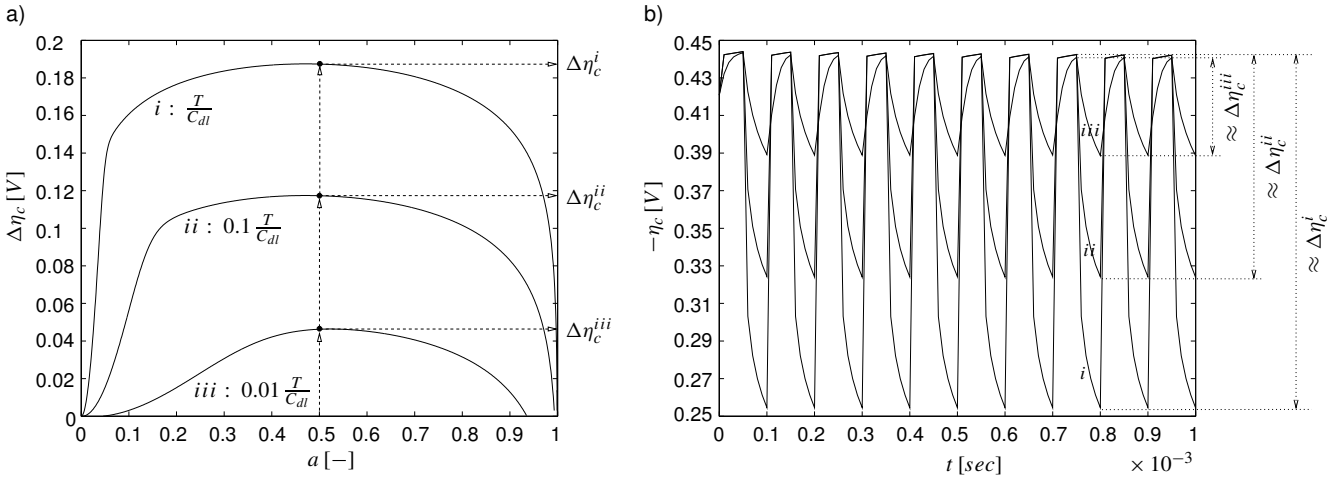

decreasing ratio of T/C_{dl} leads to smaller oscillations in the overpotential and vice versa. Therefore, in order to reduce oscillations in the fuel cell either the duty period T of the buck converter has to be

decreased or the double layer capacitance C_{dl} of the PEMFC has to be increased or both things have to be done. As was discussed in section 4.1., this can be achieved either by adjusting the switching period of the converter or by adding a capacitor. In Figure 13b an increased double layer capacitance is used. Stationary simulation results of the overpotential η_c for the coupled PEMFC and buck converter model at a duty ratio $a = 0.5$ are shown. The duty period T is held constant and the double layer capacitance is increased from its nominal value in case i to $10C_{dl}$ in case ii and $100C_{dl}$ in case iii. One can see, that the oscillation amplitudes of the overpotential decrease ($\Delta\eta_c^i > \Delta\eta_c^{ii} > \Delta\eta_c^{iii}$) as it is predicted in Figure 13a.

The oscillations in the overpotential due to the coupling of PEMFC and buck converter may also be used to estimate parameters of the fuel cell. This may be useful for monitoring or control purposes of the PEMFC. Rather expensive to obtain are the parameters describing the reaction kinetics of the fuel cell. Their identification is usually done in experiments using the impedance spectroscopy, the current interrupt technique [21] and the electrochemical parameter identification [22]. Equation (29) may also be used for this purpose. For an estimation of the fuel cell's reaction kinetics the exchange current density together with the cell's oxygen content $i_r^0\,\overline{x}_{o_2}$, the exponent in the Tafel equation $\hat{\alpha}$ and the double layer capacitance C_{dl} have to be determined. If we want to identify these parameters from Eqn. (29) we need to know the average inductor current $\overline{I}_l$ and the oscillation amplitude $\Delta\eta_c$ of the overpotential while the other quantities are rather well known. The quantity $\overline{I}_l$ can be obtained by measuring and averaging the inductor current. The oscillation amplitude $\Delta\eta_c$ can be obtained by measuring the oscillation amplitude ΔU_e of the cell voltage. If the fuel cell is well humidified the ohmic and concentration losses are negligible and we have $\Delta\eta_c \approx \Delta U_e$.

If $\overline{I}_l$ and $\Delta\eta_c$ are known we have to analyze the sensitivity of these measurements with respect to the unknown parameters in Eqn. (29) to get an indication about the quality of the obtainable estimation results. For the double layer capacitance C_{dl} we can use Figure 13 for this purpose. If we define the changes of the oscillation amplitude $\Delta\eta_c$ with respect to changes in C_{dl} at some fixed duty ratio a as sensitivity $|\Delta(\Delta\eta_c)/\Delta C_{dl}|_a$ we can see from Figure 13a that this sensitivity should be large enough for all duty ratios to get acceptable estimation results for C_{dl}. The sensitivity with respect to the exchange current density i_r^0 is analyzed in Figure 14. If we consider the changes of the oscillation amplitude $\Delta\eta_c$ with respect to the changes in i_r^0 at some duty ratio a as sensitivity $|\Delta(\Delta\eta_c)/\Delta i_r^0|_a$ it can be seen, that this sensitivity is rather small. Therefore, we cannot expect to get acceptable estimation results for $i_r^0\,\overline{x}_{o_2}$ from Eqn. (29).

Finally, in Figure 15 the sensitivity with regard to the parameter $\hat{\alpha}$ (Eqn. (4)) is examined. If we consider the changes of the stationary oscillation amplitude $\Delta\eta_c$ with respect to the changes in $\hat{\alpha}$ at a duty ratio a as sensitivity $|\Delta(\Delta\eta_c)/\Delta\hat{\alpha}|_a$ it can be seen from Figure 15, that this sensitivity should be large enough for duty ratios between 0.1 and 0.9 to get acceptable estimation results for the parameter $\hat{\alpha}$. The estimation results for $\hat{\alpha}$ can be used to determine the transfer coefficient α from Eqn. (4), since the relative change of ± 0.4 in $\hat{\alpha}$ corresponds to a relative change of ∓ 0.2 in the transfer coefficient. To determine α from Eqn. (4) the cell temperature Θ has to be roughly known, e.g. from measurements. In summary, the sensitivity analysis reveals that acceptable estimation results can be expected for the double layer capacitance C_{dl} and the parameter $\hat{\alpha}$. The exchange current density cannot be estimated due to its small sensitivity. It should be noted, that due to this fact the precise value of the exchange current density as well as the precise value of the oxygen content in the cathodic catalyst is not necessary

Figure 14. Stationary oscillation amplitudes $\Delta\eta_c$ of the overpotential with respect to the buck converter's duty ratio a at different exchange current densities i_r^0.

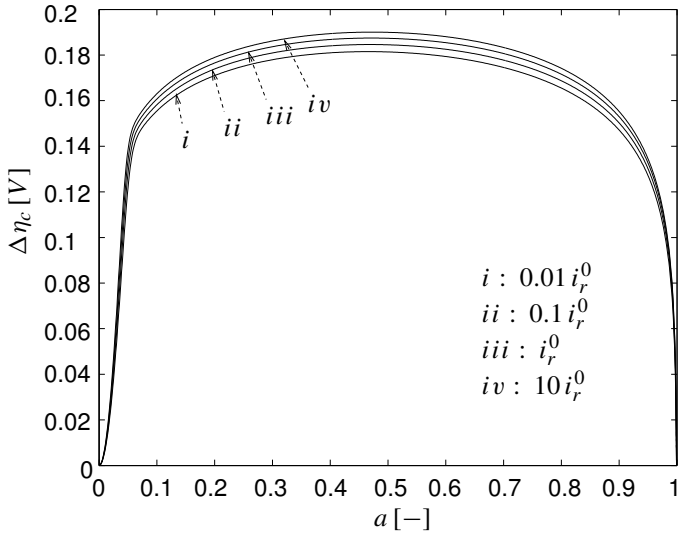

Figure 15. Stationary oscillation amplitudes $\Delta\eta_c$ of the overpotential with respect to the buck converter's duty ratio a at different values of $\hat{\alpha}$.

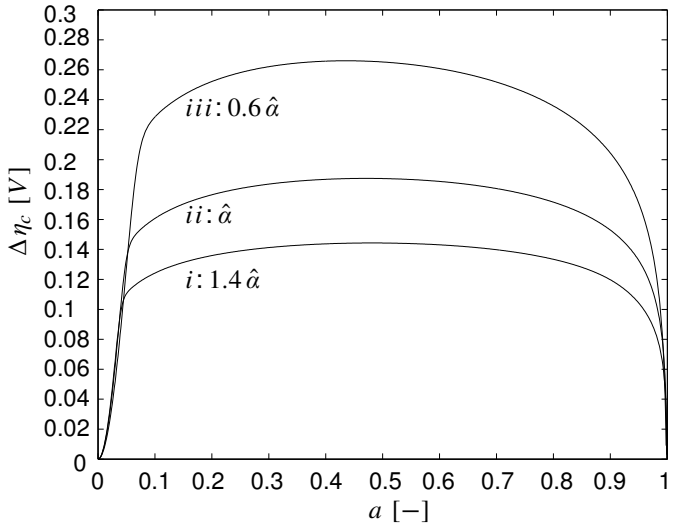

for an estimation of C_{dl} and $\hat{\alpha}$. The estimation requires the measurement of the average inductor current and the oscillation amplitude of the cell voltage at a highly humidified fuel cell. It should not be carried out at too small oscillation amplitudes $\Delta\eta_c$ to reduce the impact of the neglected inductor current ripple in Eqn. (29).

Overall behavior of the coupled system If we suppress the oscillations in the fuel cell and neglect the impact of the buck converter ripple, we can describe and analyze the coupling between the PEMFC and the buck converter with averaged model equations in order to check the overall behavior of the coupling for the appearance of stationary multiplicities and oscillations.

First of all, the stationary operation of PEMFC and buck converter is considered. Therefore, the stationary and averaged relationship in Figure 6 for the buck converter is valid. Like in the case of the PEMFC and the boost converter, the same reasoning is true and therefore the coupling between PEMFC and buck converter cannot introduce further stationary multiplicities as are already present in the PEMFC. However, oscillations induced by the coupling are still possible. In order to analyze the onset of oscillations we start with the following averaged model of PEMFC and buck converter:

$$V_c\,\dot{\overline{x}}_{o_2} = -\hat{q}(1+\overline{x}_{o_2})\,\overline{i}_r + (x^{in}_{o_2} - \overline{x}_{o_2})\,V_{in}, \tag{30}$$

$$V_c\,\dot{\overline{x}}_{h_2o} = \hat{q}(2-\overline{x}_{h_2o})\,\overline{i}_r + (x^{in}_{h_2o} - \overline{x}_{h_2o})\,V_{in}, \tag{31}$$

$$C_{dl}\,\dot{\overline{\eta}}_c = \overline{i}_r - a\,\overline{I}_l/A_g \quad \text{with} \quad \overline{i}_r = i^0_r\,\overline{x}_{o_2}\,\exp(-\hat{\alpha}\overline{\eta}_c), \tag{32}$$

$$L\,\dot{\overline{I}}_l = a\left(U^0_{cell} + \overline{\eta}_c - r_m(\overline{x}_{h_2o})\,a\,\overline{I}_l/A_g\right) - \overline{U}_c, \tag{33}$$

$$C\,\dot{\overline{U}}_c = \overline{I}_l - \overline{U}_c/R_L. \tag{34}$$

It is derived by coupling the model equations of the PEMFC (1-3) and the buck converter (8,9) via Eqn. (13) and averaging the resulting equations over one duty cycle. This is done in the same way as for the boost converter above. Like there, we consider the equations for the mass transport (30,31) as static and use only the averaged model equations (32-34). The Jacobian matrix of these equations evaluated at the steady state $(\overline{x}^{ss}_{o_2}, \overline{x}^{ss}_{h_2o}, \overline{\eta}^{ss}_c, \overline{I}^{ss}_l, \overline{U}^{ss}_c, R^{ss}_L, a_{ss})$ is given by

$$\mathbf{J} := \begin{bmatrix} -b_{11} & -b_{12} & 0 \\ b_{21} & -b_{22} & -b_{23} \\ 0 & b_{32} & -b_{33} \end{bmatrix} = \begin{bmatrix} -\hat{\alpha}a_{ss}\overline{I}^{ss}_l/A_gC_{dl} & -a_{ss}/A_gC_{dl} & 0 \\ a_{ss}/L & -a^2_{ss}r_m(\overline{x}^{ss}_{h_2o})/A_gL & -1/L \\ 0 & 1/C & -1/R^{ss}_LC \end{bmatrix}. \tag{35}$$

The duty ratio for a buck converter is typically between $0 < a_{ss} \leq 1$. With this, the coefficients b_{ij} in $\mathbf{J}$ are always positive and therefore the same reasoning as in the previous analysis of PEMFC and boost converter is true: The connection between a PEMFC and a buck converter cannot introduce a Hopf bifurcation in the coupled PEMFC - buck converter system.

4.3. PEMFC and Buck-Boost-Converter

In this section the coupling between the PEMFC and the buck-boost converter is examined.

Effect of the converter ripple upon the PEMFC In a first step the effect of the converter ripple upon the fuel cell is considered by analyzing the coupled system of switched differential equations made up

from the PEMFC (Eqns. (1-3)) and the switched buck-boost converter model (Eqns. (10,11)). The analysis reveals that the buck-boost converter introduces oscillations in the fuel cell in the same way as the buck converter. As in this previous case, the reason is due to the presence of the switching function s in the coupling of the fuel cell and the buck-boost converter: $i_{cell} = s\, I_l / A_g$. This leads to the same switched ODE for the overpotential (28) and causes the oscillations in the fuel cell.

Discussion of the effect The formula for the oscillation amplitude $\Delta\eta_c$ in Eqn. (29) can also be used to describe the stationary oscillations introduced by a buck-boost converter. Figure 16 shows the oscillation amplitude of the overpotential calculated with this formula at different duty ratios. The ratio of the duty period and the double layer capacitance T/C_{dl} is used as parameter. The load resistance R_L is set to $7\,\Omega$ while the other quantities remain constant at their nominal values. It can be seen from Figure 16,

Figure 16. Stationary oscillation amplitudes of the overpotential with respect to the buck-boost converter's duty ratio a at different ratios of duty period and double layer capacitance T/C_{dl}. The quantity $a(P_{max})$ denotes the duty ratio at the maximal cell power P_{max}.

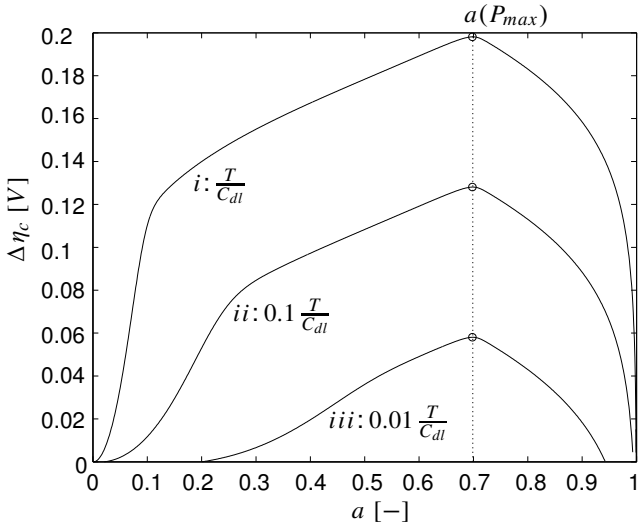

that a decreasing ratio of T/C_{dl} leads to smaller oscillations in the overpotential and vice versa. This is the same qualitative behavior as in the case of the buck converter in section 4.2.. Therefore, the same possibilities to reduce the oscillations are applicable.

The connection between the PEMFC and the buck-boost converter can also be used to estimate parameters of the fuel cell. We can use Eqn. (29) for this purpose again. In detail, the double layer capacitance C_{dl} and the exponent of the Tafel kinetics $\hat{\alpha}$ can be estimated. In the case of the double layer capacitance this can be seen from Figure 16. The sensitivity $|\Delta(\Delta\eta_c)/\Delta C_{dl}|_a$ of the oscillation amplitude with respect to the double layer capacitance should be large enough to get acceptable estimation results for C_{dl}. In the case of the parameter $\hat{\alpha}$ we can use Figure 17. We see, that the sensitivity $|\Delta(\Delta\eta_c)/\Delta\hat{\alpha}|_a$ of the oscillation amplitude $\Delta\eta_c$ with respect to $\hat{\alpha}$ should be large enough to get acceptable estimation results for $\hat{\alpha}$ too.

Figure 17. Stationary oscillation amplitudes $\Delta\eta_c$ of the overpotential with respect to the buck-boost converter's duty ratio a at different values of $\hat{\alpha}$. The quantity $a(P_{max})$ denotes the duty ratio at the maximal cell power P_{max}.

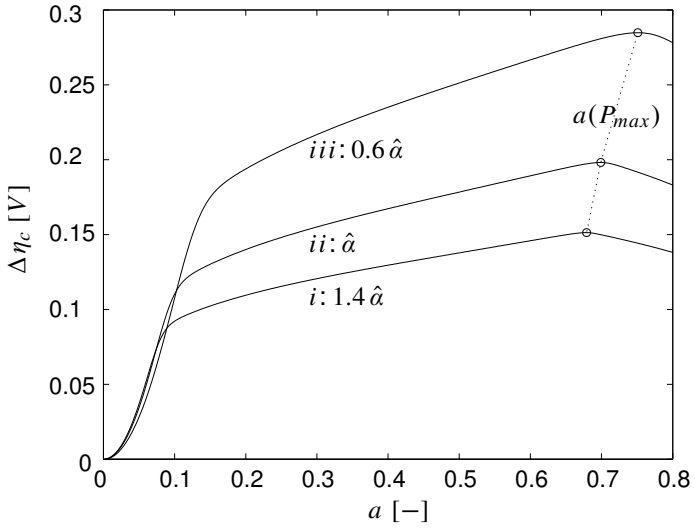

Overall behavior of the coupled system If we reduce the oscillations and are able to neglect the impact of the converter ripple we can finally analyze the overall behavior of the coupled PEMFC and buck-boost converter with averaged model equations.

First of all, the stationary operation of PEMFC and buck-boost converter is considered. Like for the previous two converters the same reasoning is true and therefore the coupling between PEMFC and buck-boost converter cannot introduce further stationary multiplicities as are already present in the PEMFC. However, oscillations are still possible and their appearance has to be analyzed. This is done by coupling and averaging the model equations of the PEMFC (1-3) and the buck-boost converter (10,11) in the same way like in the previous two cases. We obtain the same mass transport equations for oxygen and water vapor like in the case of the buck converter (Eqns. (30,31)). Like there, we assume them as static and use only the model equations for the overpotential and the buck-boost converter's inductor current and capacitor voltage:

$$C_{dl}\,\dot{\overline{\eta}}_c = i_r^0\,\overline{x}_{o_2}\,\exp(-\hat{\alpha}\overline{\eta}_c) - a\,\overline{I}_l/A_g, \tag{36}$$

$$L\,\dot{\overline{I}}_l = a\left(U_{cell}^0 + \overline{\eta}_c - r_m(\overline{x}_{h_2o})\,a\,\overline{I}_l/A_g\right) + (1-a)\overline{U}_c, \tag{37}$$

$$C\,\dot{\overline{U}}_c = -(1-a)\overline{I}_l - \overline{U}_c/R_L. \tag{38}$$

If we calculate the Jacobian matrix of the above system at the steady state $(\overline{x}_{o_2}^{ss}, \overline{x}_{h_2o}^{ss}, \overline{\eta}_c^{ss}, \overline{I}_l^{ss}, \overline{U}_c^{ss}, R_L^{ss}, a_{ss})$ we get

$$\mathbf{J} := \begin{bmatrix} -b_{11} & -b_{12} & 0 \\ b_{21} & -b_{22} & -\tilde{b}_{23} \\ 0 & \tilde{b}_{32} & -b_{33} \end{bmatrix} = \begin{bmatrix} -\hat{\alpha}a_{ss}\overline{I}_l^{ss}/A_gC_{dl} & -a_{ss}/A_gC_{dl} & 0 \\ a_{ss}/L & -a_{ss}^2 r_m(\overline{x}_{h_2o}^{ss})/A_gL & (1-a_{ss})/L \\ 0 & -(1-a_{ss})/C & -1/R_L^{ss}C \end{bmatrix}. \tag{39}$$

The duty ratio of the buck-boost converter is typically between $0 < a_{ss} < 1$. With this, the coefficients b_{ij} of $\mathbf{J}$ are always positive and the coefficients $\tilde{b}_{23}$, $\tilde{b}_{32}$ are always negative. If we calculate the characteristic

polynomial of **J** we get the equations (23-26) with negative quantities $b_{23} = \tilde{b}_{23}$ and $b_{32} = \tilde{b}_{32}$. Despite this difference, the coefficients c_0, c_1, c_2 of the characteristic polynomial and the condition $c_2c_1 - c_0$ are still positive due to the fact that only the positive product $b_{23}b_{32} = \tilde{b}_{23}\tilde{b}_{32} > 0$ enters the determining equations (24-27). Therefore, the same conclusion as in the case of the PEMFC and the boost converter applys: The connection of a PEMFC and a buck-boost converter cannot induce a Hopf bifurcation in the coupled system.

5. Conclusion

The connection of PEM fuel cells and DC-DC converters is analyzed in this contribution. The analysis is done for common DC-DC converters like the boost, buck and buck-boost converters. First of all, the effect of the converter ripples are shown. They introduce oscillations in the fuel cell. Their origin is explained, discussed and possibilities for their suppression are given. In the case of the coupling between PEMFC and buck and buck-boost converter it is shown, that the oscillations may also be useful to estimate parameter of the fuel cell's Tafel kinetic.

Finally, the overall behaviors of the coupled systems are examined. This is a necessary step, because PEM fuel cells can show a complex nonlinear behavior like multiplicities, instabilities and oscillations [18, 19, 23–25] and the coupling with DC-DC converters might have introduced additional nonlinear effects. We have shown mathematically, that this is not the case: The connection between PEM fuel cells and boost, buck and buck-boost converters can neither lead to stationary multiplicities nor to oscillations in the coupled systems. As a consequence, it is not necessary to develop integrated control approaches for the couplings. Instead, we can concentrate ourselves on the development of control strategies considering only the PEMFC and we can use existing control approaches for the DC-DC converters [7] in order to control both subsystems.

Although the PEMFC model used in this contribution is quite simple, the obtained results are also valid for PEMFC stacks in general. This due to the fact, that in PEMFC stacks the electrochemical reactions in the catalysts can also be described by the modeling approach we use in our analysis. Other transient effects that appear in PEMFC stacks, like the mass transport of gases and liquid water through the gas diffusion layers, the catalyst layers or the membrane as well as the transient behavior of the operating temperature of the fuel cell are orders of magnitudes slower than the electrochemical processes and can therefore be neglected.

Acknowledgment

The authors thank Prof. Lindemann for helpful discussions.

A Derivation of the PEMFC model

In this section the equations for the fuel cell model are derived. At first, this is done for the differential equation of the overpotential from the equivalent electrical circuit in Figure 1. The charge balance at the double layer capacitor C_{dl} reads $dQ/dt = i_c = i_{cell} - i_r$. The charge Q can be expressed in terms of the overpotential to be $Q = -C_{dl}\,\eta_c$ where $\eta_c < 0$. If the double layer capacitance is assumed to be constant

and the current i_r is expressed using the Tafel equation

$$i_r = i_r^0 x_{o_2} exp(-\hat{\alpha}\eta_c) \quad \text{with} \quad \hat{\alpha} := (1-\alpha)nF \,/\, R\Theta\,, \tag{40}$$

the differential equation for the overpotential in Eqn. (3) results. The algebraic equation for the cell voltage in Eqn. (5) can be obtained using Kirchhoff's voltage law.

The model equations for the oxygen and water content in the fuel cell are derived from the CSTR in Figure 1. Mass balances for the species $k \in \{O_2, N_2, H_2O\}$ read

$$\dot{n}_k = V_{in} c_k^{in} - V_{out} c_k + \nu_k r A_g \tag{41}$$

where n_k (c_k) describes the molar amount (concentration) of species k in the CSTR. The symbol ν_k denotes the stoichiometric coefficients of the cathodic reaction with $\nu_{o_2} = -0.5$, $\nu_{h_2o} = 1$ and $\nu_{n_2} = 0$ and the quantity r refers to the reaction rate and is given by Faraday's law $r = i_r/nF$. The volume flow rate of air at the inlet V_{in} is kept constant. The volume flow rate at the output V_{out} can be determined if the gas phase is assumed to be isotherm, isobaric and ideal. The ideal gas law reads $p_g V_c = n_{all} R\Theta$. The symbol $n_{all} = \sum_k n_k$ denotes the whole amount of gas inside the CSTR and is constant if isobaric, isothermic conditions as well as a constant CSTR volume V_c is assumed. This means $\dot{n}_{all} = \sum_k \dot{n}_k = 0$. If the mass balances from Eqn. (41) are inserted an algebraic equation for the output flow rate V_{out} results: $V_{in} \sum_k c_k^{in} - V_{out} \sum_k c_k + \sum_k \nu_k r A_g = 0$. This equation can be simplified if the total concentration in the CSTR $c_t := n_{all}/V_c = \sum_k n_k/V_c = \sum_k c_k = p_g/R\Theta = const.$ is defined. The total concentration in the CSTR and the inlet is the same: $c_t^{in} = c_t$ because we assume an ideal and isobaric, isothermic gas phase in the inlet as well. With these simplifications the output flow rate can be written as

$$V_{out} = V_{in} + \sum_k \nu_k A_g r/c_t = V_{in} + A_g i_r / 2 c_t nF\,. \tag{42}$$

If we insert the above equation in Eqn. (41) and use $n_k = V_c\, c_k$ and molar fractions $x_k := n_k/n_{all} = c_k/c_t$, $x_k^{in} = c_k^{in}/c_t$ the model equations (1,2) result for $k = O_2, H_2O$.

B Enlargement of the double layer capacitance

In this section it is briefly shown that a capacitor connected in parallel to a PEMFC can be used to increase the double layer capacitance of the cell. The capacitor with capacitance C_{II} is assumed to be lossless and is connected to the ports of the equivalent electrical circuit in Figure 1. The capacitor can be used to suppress oscillations in the fuel cell induced by the duty cycle of a connected DC/DC-converter. A time interval of one duty period T is considered for the following equations. For the overpotential η_c and the cell voltage U_{cell} the Eqns. (3,5) are still valid. The voltage at the new capacitor is identical to the cell voltage and is calculated by

$$C_{II} \frac{dU_{cell}}{dt} = i_{cell} - i\,, \tag{43}$$

where i denotes the new output current of the fuel cell that is different from i_{cell}. If Eqn. (5) is differentiated with respect to time and inserted in Eqn. (43) one gets

$$C_{II} \left(\frac{d\eta_c}{dt} - r_m \frac{di_{cell}}{dt} \right) = i_{cell} - i\,, \tag{44}$$

where we have assumed, that the change in water content x_{h_2o} in the cell is negligible over one duty period. If Eqn. (3) is differentiated with respect to time under the assumption that the oxygen content x_{o_2} is assumed to be constant and solved for di_{cell}/dt we obtain

$$\frac{di_{cell}}{dt} = \frac{\partial i_r}{\partial \eta_c}\frac{d\eta_c}{dt} - C_{dl}\frac{d^2\eta_c}{dt^2}\,. \tag{45}$$

where i_r denotes the Tafel equation (40). If Eqn. (45) and Eqn. (3) are inserted for di_{cell}/dt and i_{cell} in Eqn. (44) a second order ODE for the overpotential results:

$$r_m C_{dl} C_{II}\frac{d^2\eta_c}{dt^2} + \left(C_{dl} + C_{II}\left[1 - r_m\frac{\partial i_r}{\partial \eta_c}\right]\right)\frac{d\eta_c}{dt} = i_r(\eta_c) - i\,. \tag{46}$$

If the first term on the left hand side is negligible compared to the second term, e.g. if the fuel cell is well humidified and leads to a fairly small membrane resistance r_m, a first order ODE for the overpotential follows:

$$\left(C_{dl} + C_{II}\left[1 + r_m\,\hat{\alpha}\,i_r(\eta_c)\right]\right)\frac{d\eta_c}{dt} = i_r(\eta_c) - i\,. \tag{47}$$

This equation has the same structure as the original ODE for the overpotential in Eqn. (3) whereas the new equation and therefore the parallel connection of the fuel cell and the capacitor shows an increased double layer capacitance.

C Formula for stationary oscillations of the overpotential in a PEMFC if connected to buck or buck-boost converters

In this section the formula in Eqn. (29) is derived. The ODE for the overpotential in Eqn. (28) is used as a starting point. It is assumed that the changes in the inductor current I_l and the oxygen content x_{o_2} are small over one duty period T of the converter and can be approximately replaced by their average values $\overline{I}_l$ and $\overline{x}_{o_2}$. If the switching function s is defined by

$$s = \begin{cases} 1 & , \quad t \in \mathfrak{T}_{on} := [t_0, t_0 + t_{on}[\\ 0 & , \quad t \in \mathfrak{T}_{off} := [t_0 + t_{on}, t_0 + T[\end{cases} \tag{48}$$

the following nonlinear ODE in η_c results:

$$C_{dl}\,\dot{\eta}_c = \begin{cases} -\frac{\overline{I}_l}{A_g} + i_r^0\overline{x}_{o_2}\exp(-\hat{\alpha}\eta_c) & , \quad t \in \mathfrak{T}_{on} \\ i_r^0\overline{x}_{o_2}\exp(-\hat{\alpha}\eta_c) & , \quad t \in \mathfrak{T}_{off} \end{cases} \tag{49}$$

with initial conditions $\eta_c(t_0) = \eta_{c_0}$ and $\eta_c(t_0 + t_{on}) = \eta_{c_1}$. With the following change in variables $z := \exp(\hat{\alpha}\eta_c)$ and the definitions $\beta := \hat{\alpha}\,\overline{I}_l/A_g\,C_{dl}$ and $\gamma := \hat{\alpha}\,i_r^0\,\overline{x}_{o_2}/C_{dl}$ a linear ODE in z can be obtained:

$$\dot{z} = \begin{cases} -\beta\,z + \gamma & , \quad t \in \mathfrak{T}_{on} \\ \gamma & , \quad t \in \mathfrak{T}_{off} \end{cases} \tag{50}$$

This ODE can be solved easily and the solution in the original variables reads

$$\eta_c^{on} = \frac{1}{\hat{\alpha}}\ln\left(\frac{\gamma}{\beta} + \left(\exp(\hat{\alpha}\,\eta_{c_0}) - \frac{\gamma}{\beta}\right)\exp(-\beta(t - t_0))\right)\,,\ t \in \mathfrak{T}_{on} \tag{51}$$

$$\eta_c^{off} = \frac{1}{\hat{\alpha}}\ln\left(\exp(\hat{\alpha}\,\eta_{c_1}) + \gamma(t - (t_0 + t_{on}))\right)\,,\ t \in \mathfrak{T}_{off}\,. \tag{52}$$

With the above solutions we can now define the oscillation amplitude $\Delta\eta_c$ of the overpotential. It is given by

$$\Delta\eta_c := \lim_{t\to t_0+T} \eta_c^{off} - \lim_{t\to t_0+t_{on}} \eta_c^{on} \tag{53}$$

with unknown initial conditions η_{c_0} and η_{c_1}. The initial condition η_{c_1} can be calculated by demanding continuity at $t = t_0 + t_{on}$ between both solutions: $\eta_{c_1} \triangleq \lim_{t\to t_0+t_{on}} \eta_c^{on}$. We get from Eqn. (51)

$$\exp(\hat{\alpha}\,\eta_{c_1}) = \frac{\gamma}{\beta} + \left(\exp(\hat{\alpha}\,\eta_{c_0}) - \frac{\gamma}{\beta}\right) \exp(-\beta\,t_{on})\,. \tag{54}$$

The initial condition η_{c_0} can be obtained by demanding $\eta_{c_0} \triangleq \lim_{t\to t_0+T} \eta_c^{off}$. This is valid for the stationary case and we get

$$\exp(\hat{\alpha}\,\eta_{c_0}) = \frac{(\frac{\gamma}{\beta})^2 \exp(-\beta\,t_{on}) - \gamma(T - t_{on})}{\frac{\gamma}{\beta}\exp(-\beta\,t_{on}) - 1} \tag{55}$$

from calculating this limit from Eqn. (52) after inserting Eqn. (54). The initial conditions in the solutions can now be eliminated by inserting Eqns. (54,55) in Eqns. (51,52). Therefore, the stationary oscillation amplitude of the overpotential can now be calculated from Eqn. (53). With the relation $a = t_{on}/T$ from Eqn. (12) the formula in Eqn. (29) results. Note that the oscillation amplitude $\Delta\eta_c = \eta_{c_0} - \eta_{c_1}$ has to be always greater than zero, because in fuel cell operation we have $\eta_{c_0} > \eta_{c_1}$. With Eqns. (54,55) and $a = t_{on}/T$ this condition can be reformulated to $(1 - a)\,T\,\beta > 1$.

Nomenclature

α transfer coefficient of cathodic reaction, 0.5

η_c overvoltage at cathodic catalyst, V

σ_p proton conductivity of membrane, Sm^{-1}

σ_{p_0} min. proton conductivity of membrane, $1.3 \times 10^{-5}\,Sm^{-1}$

Θ cell temperature, $353\,K$

a duty ratio of DC-DC converters

A_g cross-sectional area of fuel cell, $1.0 \times 10^{-4}\,m^2$

C capacitance of DC-DC converters, $300.0 \times 10^{-6}\,F$

c_t $p_g/(R\Theta)$, $molm^{-3}$

C_{dl} double layer capacitance, $0.01\,Fm^{-2}$

d_m membrane thickness, $25 \times 10^{-6}\,m$

F Faraday constant, $96485.3\,Cmol^{-1}$

I_e input current of DC-DC converters, A

I_l inductor current of DC-DC converters, A

i_r^0 exchange current density, $0.01\ Am^{-2}$

i_{cell} cell current density, Am^{-2}

L inductivity of DC-DC converters, $82.0 \times 10^{-5}\ H$

n number of electrons consumed in cathodic reaction, 2

p_g overall gas pressure, $1.013 \times 10^5\ Pa$

p_{sat} saturation pressure of H_2O at Θ, $4.7373 \times 10^4\ Pa$

R gas constant, $8.314 Jmol^{-1}\ K^{-1}$

R_L resistive load of DC-DC converters, Ω

r_m membrane resistance against proton transport, Ωm^2

T duty period of DC-DC converters, $1.0 \times 10^{-4}\ s$

U_c capacitor (=output) voltage of DC-DC converters, V

U_{cell} cell voltage, V

U_{cell}^0 equilibrium voltage of the cell, $1.17\ V$

V_c gas volume of CSTR, $0.5 \times 10^{-6}\ m^3$

V_{in} volume flow rate of air, $1.7873 \times 10^{-7}\ m^3 s^{-1}$

x_{h_2o} molar fraction of H_2O

$x_{h_2o}^{in}$ molar fraction of H_2O at inlet, 0.14

x_{o_2} molar fraction of O_2

$x_{o_2}^{in}$ molar fraction of O_2 at inlet, 0.21

References and Notes

1. Choi, W.; Howze, J.; Enjeti, P. Development of an equivalent circuit model of a fuel cell to evaluate the effects of inverter ripple current. *J. Power Sources* **2006**, *158*, 1324–1332.
2. Gemmen, R. S. Analysis for the effect of inverter ripple current on fuel cell operating condition. *Trans. ASME* **2003**, *125*, 576–585.
3. Shireen, W.; Kulkarni, R. A.; Arefeen, M. Analysis and minimization of input ripple current in pwm inverters for designing reliable fuel cell power systems. *J. Power Sources* **2006**, *156*, 448–454.
4. Zenith, F.; Skogestad, S. Control of fuel cell power output. *J. Proc. Control* **2007**, *17*, 333–347.

5. Eikerling, M.; Kornyshev, A. A. Electrochemical impedance of the cathode catalyst layer in polymer electrolyte fuel cells. *J. Electroanalyt. Chem.* **1999**, *475*, 107–123.
6. Ziegler, C.; Yu, H.; Schumacher, J. Two-phase dynamic modeling of the PEMFC and simulation of cyclo-voltammograms. *J. Electrochem. Soc.* **2005**, *152*, A1555–A1567.
7. Erickson, R. W.; Maksimović, D. *Fundamentals of Power Electronics*; Springer-Verlag: Heidelberg, Germany, 2001.
8. Seifart, M. *Analoge Schaltungen*; Verlag Technik, 2003 (in German).
9. Yang, C.; Srinivasan, S.; Bocarsly, A. B.; Tulyani, S.; Benziger, J. B. A comparison of physical properties and fuel cell performance of nafion and zirconium phosphate/nafion composite membranes. *J. Membrane Sci.* **2004**, *237*, 145–161.
10. Barbir, F. *PEM Fuel Cells*; Academic Press Sustainable World, Elsevier: Amsterdam, The Netherlands, 2005.
11. Ziegler, C.; Schmitz, A.; Tranitz, M.; Fontes, E.; Schumacher, J. O. Modeling planar and self-breathing fuel cells for use in electronic devices. *J. Electrochem. Soc.* **2004**, *151*, A2028–A2041.
12. de Bruijn, F.; Dam, V.; Janssen, G. Review: Durability and Degradation Issues of PEM Fuel Cell Components. *Fuel Cells* **2008**, *8*, 3–22.
13. Bautista, M.; Bultel, Y.; Ozil, P. Polymer electrolyte membrane fuel cell modelling: d.c. and a.c. solutions. *Chem. Eng. Res. Design* **2004**, *82*, 907–917.
14. Bultel, Y.; Wiezell, K.; Jaouen, F.; Ozil, P.; Lindbergh, G. Investigation of mass transport in gas diffusion layer at the air cathode of a pemfc. *Electrochim. Acta* **2005**, *51*, 474–488.
15. Makharia, R.; Mathias, M. F.; Baker, D. R. Measurement of catalyst layer electrolyte resistance in pefcs using electrochemical impedance spectroscopy. *J. Electrochem. Soc.* **2005**, *152*, A970–A977.
16. Rubio, M.; Urquia, A.; Dormido, S. Diagnosis of pem fuel cells through current interruption. *J. Power Sources* **2007**, *171*, 670–677.
17. Benziger, J.; Chia, E.; Moxley, J.; Kevrekidis, I. The dynamic response of pem fuel cells to changes in load. *Chem. Eng. Sci.* **2005**, *60*, 1743–1759.
18. Grötsch, M.; Hanke-Rauschenbach, R.; Mangold, M. Bifurcation analysis of a two-phase pemfc model. *J. Fuel Cell Sci. Technol.* **2008**, *5*, 021001–021009.
19. Hanke-Rauschenbach, R.; Mangold, M.; Sundmacher, K. Bistable current-voltage characteristics of pem fuel cells operated with reduced feed stream humidification. *J. Electrochem. Soc.* **2008**, *155*, B97–B107.
20. Ludyk, G. *Theoretische Regelungstechnik 1*; Springer-Verlag: Heidelberg, Germany, 1995 (in German).
21. Schindele, L. Einsatz eines leistungselektronischen Stellglieds zur Parameteridentifikation und optimalen Betriebsführung von PEM-Brennstoffzellensystemen. Ph.D. thesis, University Karlsruhe, Germany, 2006 (in German).
22. Danzer, M.; Hofer, E. Electrochemical parameter identification - an efficient method for fuel cell impedance characterisation. *J. Power Sources* **2008**, *183*, 55–61.
23. Kulikovsky, A. A. The effect of stoichiometric ratio [lambda] on the performance of a polymer electrolyte fuel cell. *Electrochim. Acta* **2004**, *49*, 617–625.
24. Zhang, J.; Fehribach, J. D.; Datta, R. Mechanistic and bifurcation analysis of anode potential oscillations in pemfcs with co in anode feed. *J. Electrochem. Soc.* **2004**, *151*, A689–A697.

25. Katsaounis, A.; Balomenou, S.; Tsiplakides, D.; Brosda, S.; Neophytides, S.; Vayenas, C. Proton tunneling-induced bistability, oscillations and enhanced performance of pem fuel cells. *Appl. Catal. B: Environ.* **2005**, *56*, 251–258.